Effect of Surface Pretreatment on the Underpaint Corrosion of AA2024-T3 at Various Temperatures

D.A. Little,* M.A. Jakab,*,** and J.R. Scully‡,*

ABSTRACT

The effects of surface pretreatment on the rate of scribe-creep caused by underpaint corrosion on coated AA2024-T3 (UNS A92024) were investigated. Scribe-creep experiments were conducted on epoxy polyamide-coated (average coating thickness: ~10 μm) AA2024-T3 in 80% relative humidity at 25°C, 40°C, and 50°C. Scribe-creep was observed to be enhanced by exposure test temperature regardless of surface pretreatment with an activation energy of 30 kJ/mol to 40 kJ/mol. The scribe-creep rate was accelerated at all temperatures especially by pretreatments that increased the concentration of surface Cu or left a high capacity for Cu-replating. Sodium hydroxide (NaOH) etching particularly increased the amount of replated Cu at the coated metal interface compared with an as-received condition and a NaOH etch followed by a nitric acid (HNO_3) deoxidation. The effect of each surface pretreatment to enhance or retard scribe-creep is traced either to the initial level of Cu replating prior to coating or to its ability to supply Cu for replating in the scribe-creep filament wake. This Cu replating enhances the rate of cathodic electron transfer reactions, which supports the galvanic corrosion process between scribe-creep head and tail. When Cu was eliminated as an alloying element, or when surface Cu was minimized at the coating-metal interface by HNO_3 deoxidation pretreatment, scribe-creep corrosion rates were lowered. This was rationalized to occur as a result of a decrease in the cathodic oxygen reduction reaction rate, which supports anodic undercutting at the head of the corrosion front.

Submitted for publication December 2004; in revised form, June 2005.

‡ Corresponding author. E-mail: jrs8d@virginia.edu.
* University of Virginia, 116 Engineers Way, Charlottesville, VA 22904.
** Current address: Southwest Research Institute, 6220 Culebra Rd., San Antonio, TX 78228.

(1) UNS numbers are listed in *Metals and Alloys in the Unified Numbering System*, published by the Society of Automotive Engineers (SAE International) and cosponsored by ASTM International.

KEY WORDS: copper replating, filiform corrosion, surface pretreatments, underpaint corrosion

INTRODUCTION

Al-based precipitation age-hardened alloys containing Cu and Fe are prone to localized corrosion such as pitting induced by galvanic interactions between Cu-rich intermetallic compounds (IMC) and the Al alloy matrix. These local galvanic cells, which induce acid pitting and alkaline attack, are often formed by Cu- and Fe-containing intermetallics or replated Cu.[1-12] In AA2024-T3 (UNS A92024),[(1)] pit initiation sites include Al-Cu-Mg particles,[2-3,7,11-13] the periphery of Cu-enriched Al-Cu-Mg particles that have been dealloyed of Al and Mg,[2] and the matrix adjacent to Al-Cu and Al-Cu-Fe-Mn constituent particles.[3,5,10,13] The Al-Cu-Mg type is the most active constituent particle and as much as 60% of the intermetallics on the surface of an AA2024-T3 sample are of the Al-Cu-Mg type,[2,14-15] with 2.7% of the total surface covered by these particles.[2] The Al-Cu-Mg type IMC is anodic to the Al alloy matrix and is present as 1-μm to 10-μm-diameter particles.[16] The smaller particles will dissolve completely, while the larger particles generally undergo selective dissolution of the Al and Mg from the particle, leaving only a fine Cu sponge.[2-3,12,15,17-18] The particle becomes cathodic to the matrix with time.[2-3,11-12,19-20] Under certain conditions, some authors have observed rings of deposited Cu around these Al-Cu-Mg precipitates, suggesting that they are a major source of Cu for replating.[18] The Al-Cu and Al-Cu-Mn-Fe types of IMC also serve as preferred cathodic sites relative to the Al matrix.[21] Cu^{2+} ions dissolved into solution can be reduced readily on these particles and elsewhere.[3] The

0010-9312/06/000059/$5.00+$0.50/0
© 2006, NACE International

generation of OH^- ions at these particles due to the reduction of oxygen is believed to contribute to alkaline attack of the Al adjacent to these particles, resulting in an attack morphology known as trenching, which often forms a perimeter around the particle.[3-4,6,10,13,20] Recent work, however, suggests other mechanisms for trenching.[22] In addition, pitting can occur in the matrix in halide-containing solutions.[21] Cu-rich IMC and replated Cu have been shown to contribute significantly to the overall oxygen reduction reaction (ORR) rate on AA2024-T3.[18,20-21,23-29] Therefore, a cathodic reaction is readily available from a coating defect in the case of underpaint corrosion to support the operating anodic corrosion process at the head of a coating delamination front.

Few studies have addressed the role of Al-precipitation age-hardened alloy microstructure and composition on the progression of the corrosion-related events leading to organic coating degradation from either macroscopic coating defects or intact coatings. It is clear that underpaint corrosion initiates at paint defects that expose the underlying microstructure. Underpaint corrosion in Al alloys most likely occurs through anodic wedging[30] and anodic undercutting.[31-34] According to this mechanism the head and tail form the anode and cathode, respectively. These anode/cathode positions have been confirmed by scanning Kelvin probe measurements at the sites where scribe-creep was observed under polyvinyl butyral-co-vinyl alcohol-co-vinyl acetate coatings on steel[35-36] and commercial polymer coatings on AA2024-T3.[37] Model Al-Cu alloys were created by depositing a regular array of Cu islands on high-purity Al.[38] When coated with an organic polymer coating, micron-scale pitting at Cu dots transitioned to the formation of mm-scale, low-pH anodes at the filiform tip, and high-pH cathodes at filiform tails.[38] However, there are few studies that link the specific behavior and roles of actual microstructural features, such as constituent particles in Al-Cu precipitation age-hardened alloys, or pretreatments that affect microstructural features, to the initiation or propagation stages of corrosion under organic coatings on Al-based alloys.[39]

Information available suggests that alloy composition, particularly Cu and Fe content, have a dominant effect on filiform growth rates when grown from physical scratches.[40-41] Filiform corrosion (FFC) is known to proceed at enhanced rates on Cu-bearing Al alloys[42-43] even when chromate conversion coated.[44] FFC was also promoted on model Al substrates containing a regular distribution of Cu islands.[38] In fact, filiform tracts were arrested at the ends of the arrays of Cu dots, suggesting the importance of cathode sites that support fast electron transfer reaction (ETR) rates in close proximity to anode sites. Anodizing and conversion coatings are known to minimize but not eliminate FFC on AA2024-T3.[42] Moreover, the same surface preparation and organic coating type and thickness are known to result in drastically different undercoating corrosion rates in the Cu-containing 2000 series Al alloys compared to the 5000 series Al alloys.[45-46] Indeed, underpaint corrosion susceptibility of high Cu-containing 2xxx and 7xxx alloys is greater than that of 6xxx with lower solute content such as Cu.[40] The 5xxx alloys with nil-Cu perform even better, indicating that the overall performance of coated metals is linked to the corrosion and electrochemical properties of the substrate alloy.[47-48] Papers by Afseth, et al.,[47] and Zhou, et al.,[48] focus on the role of alloyed Mn and the effects of surface conditioning or treatment on FFC resistance. It has been shown that alkaline cleaning of the surface leads to increased FFC growth rates. Decreased severity of attack occurs in the filament tail when deoxidizing is conducted after alkaline cleaning. Chromate conversion coatings also lead to a decrease in the FFC growth rates but increased severity of the attack is observed in the filament tail.[49-51] A decrease in rate has been related to the adhesion of the coating as a result of these surface pretreatments.[49-51] However, the effects of pretreatment that specifically alter surface Cu content in the form of IMC and replated Cu that drive cathodic electron transfer reactions (ETR) have not been investigated.

The objective of our study was to understand the role(s) of alloy composition, intermetallics, and replated Cu, mediated by pretreatment and the capacity for Cu release during the coating process, on the propagation of underpaint corrosion that results in a coating delamination process commonly referred to as scribe-creep. In this preliminary study, the effects of pretreatment on the rate of scribe-creep are investigated. The extent of Cu replating prior to coating deposition can be enhanced or reduced on AA2024-T3 by combinations of treatments such as those examined by others.[16-17] The effects of these processes on FFC processes are investigated. An organic epoxy polyamide coating consistent with that of aircraft primers was applied to AA2024-T3 and scribed.

EXPERIMENTAL PROCEDURES

The material used for this study was 1.5-mm-thick AA2024-T3 sheet with a composition (wt%) of 0.009% Cr, 4.35% Cu, 0.19% Fe, 1.36% Mg, 0.62% Mn, 0.099% Si, 0.025% Ti, 0.095% Zn, and balance Al. As was stated above, the IMC for this alloy are primarily of the Al-Cu, Al-Cu-Mg, and Al-Cu-Mn-Fe compositions.[2-3,5,7,10-15,21-22,24] Using scanning electron microscopy (SEM) and image analysis, the surface area ratio for coarse constituent-type IMC was 2.18%, with an average IMC diameter of 2.43 μm (Figure 1) after stereological correction using the Saltyov (area) method.[52-53] The L_2 statistical point pattern spatial analysis[54-55] performed on the IMC on the long transverse (LT) or rolling surface showed that the IMC are sometimes clustered and sometimes random, as can

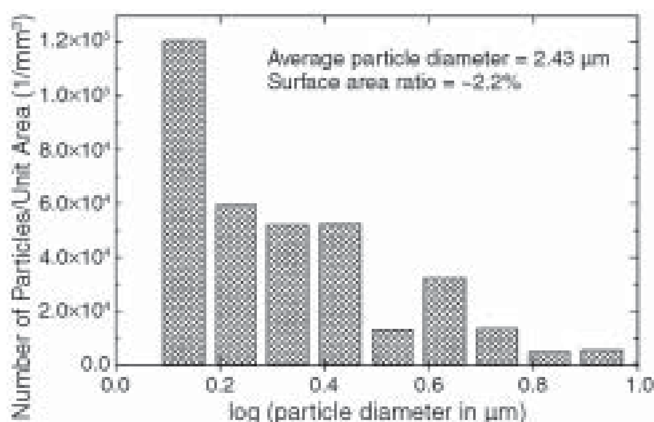

FIGURE 1. *Microstructural constituent particle size frequency for unpretreated AA2024-T3 LT surface observed from SEM backscattered electron image.*

be seen from Figure 2.[(2)] Scribe-creep tests were conducted on LT surfaces and were augmented by studies on high-purity Al (99.999%).

The AA2024-T3 sheet was cut into squares of 5 cm by 5 cm for a variety of testing purposes. All samples prepared for testing purposes were mechanically wet-ground to a surface finish of 1200 grit using silicon carbide (SiC) paper. The panels were then cleaned in water and degreased by immersing the panels in butanone for 30 s, a procedure similar to that used by others.[47,56-59] Three surface treatments were utilized on the LT surfaces of AA2024-T3 to maximize and minimize the replated Cu content for testing purposes:[47,56-59]

—a 40-min immersion in 1.5 g/L sodium hydroxide (NaOH) (alkaline etch) followed by rinsing with deionized water to etch and replate a high amount of Cu on the surface
—a 40-min immersion in 1.5 g/L NaOH, followed by rinsing with deionized water, 30-s immersion in 50 wt% nitric acid (HNO_3), and rinsing with deionized water to etch the surface, then remove the IMC from the surface to minimize the surface Cu content (NaOH + HNO_3)
—no chemical treatment of the surface

Cyclic voltammetric measurements were performed on the electrodes after these various surface pretreatments to qualitatively determine the initial amount of replated Cu prior to underpaint corrosion testing. Cyclic voltammetry has been shown to be an effective method of determining the replated Cu surface coverage or the lack thereof.[56] It has also been recently corroborated with independent measures of surface Cu detected by x-ray photoelectron spectroscopy.[60] The extent of Cu replating is a strong indicator of the extent of corrosion because it indirectly indicates the extent of IMC attack, cathodic trenching, and pitting, all of which lead to Cu release and redeposition. In the case of scribe-creep, replated Cu would increase the ability to support cathodic ETR rates that might enable faster scribe-creep rates, assuming that the process is not completely controlled by anodic reactions at the anode head.

The cyclic voltammetric tests were performed in a deaerated, pH = 8.4 borate buffer solution (8.17 g/L sodium borate [$Na_2B_4O_7 \cdot 10\ H_2O$] + 7.07 g/L boric acid [H_3BO_3]) to detect and assay surface Cu.[(3)] Specimens were held potentiostatically at –700 mV vs. saturated calomel electrode (SCE) for 5 min prior to the first cyclic voltammetric scan, held at the same potential for 10 min before the second cyclic voltammetric scan, and for 20 min before the third cyclic voltammetric scan. The cyclic voltammograms were conducted by scanning at a rate of 1 mV/s from –700 mV_{SCE} to a vertex potential of 300 mV_{SCE}, then scanning back to –1,200 mV_{SCE}. Only the last cyclic voltammetry scan was used for analysis because the background signal for Al oxidation was minimized by the third cycle. Thus, Cu oxidation/reduction peaks could be more clearly distinguished. The Cu oxidation peaks were selected for analysis of Cu levels, since they were more prominent than the reduction peaks, which were more distributed. Increasing peak height was correlated with increasing peak area.[60-61] Peak height was subsequently used. Various scans were compared to assess Cu-replating both before the coating was applied and upon removal of the coating after the humidity exposure.

Humid air exposure studies were performed on scratched, coated AA2024-T3 planar electrodes on LT surfaces. AA2024-T3 panels (5 cm by 5 cm) were tested with the same pretreatments as those used for the cyclic voltammetry scans mentioned earlier. The panels were coated with a translucent epoxy polyamide coating similar to aircraft primers. It was prepared by mixing equal weights of Epon resin 1001-CX-75† (Shell) with Epi-Cure 3115 X73† curing agent (fatty acid-polyethylene polyamine-based polyamide mixture, Shell) and adding 5 wt% Butylcellosolve. The coating was applied using a spin coater and then the coated panel was placed in a dessicator out of the light for at least one week for curing. The average coating thickness was approximately 10 µm. The backs of the coated panels were masked from the humidity exposure using electroplating tape and the sides were masked using a removable masking lacquer. Samples were scribed perpendicular to the rolling direction using a sharp scalpel that penetrated the coating on the AA2024-T3 panels and scratched through the pretreated surface of the substrate as well. The scratch was 4 cm long. Drops of 16 wt% (~5.2 M) hydrochloric acid (HCl) solution were placed along the scratch for 30 s, and then the excess acid was removed. These test coupons were then placed

[(2)] Nanometer scale precipitates were not detected using this method.
[(3)] Negligible Cu-replating was seen on the AA2024-T3 control specimens exposed only to borate buffer. Acidification and alkalinization were minimized by this choice of electrolyte.
† Trade name.

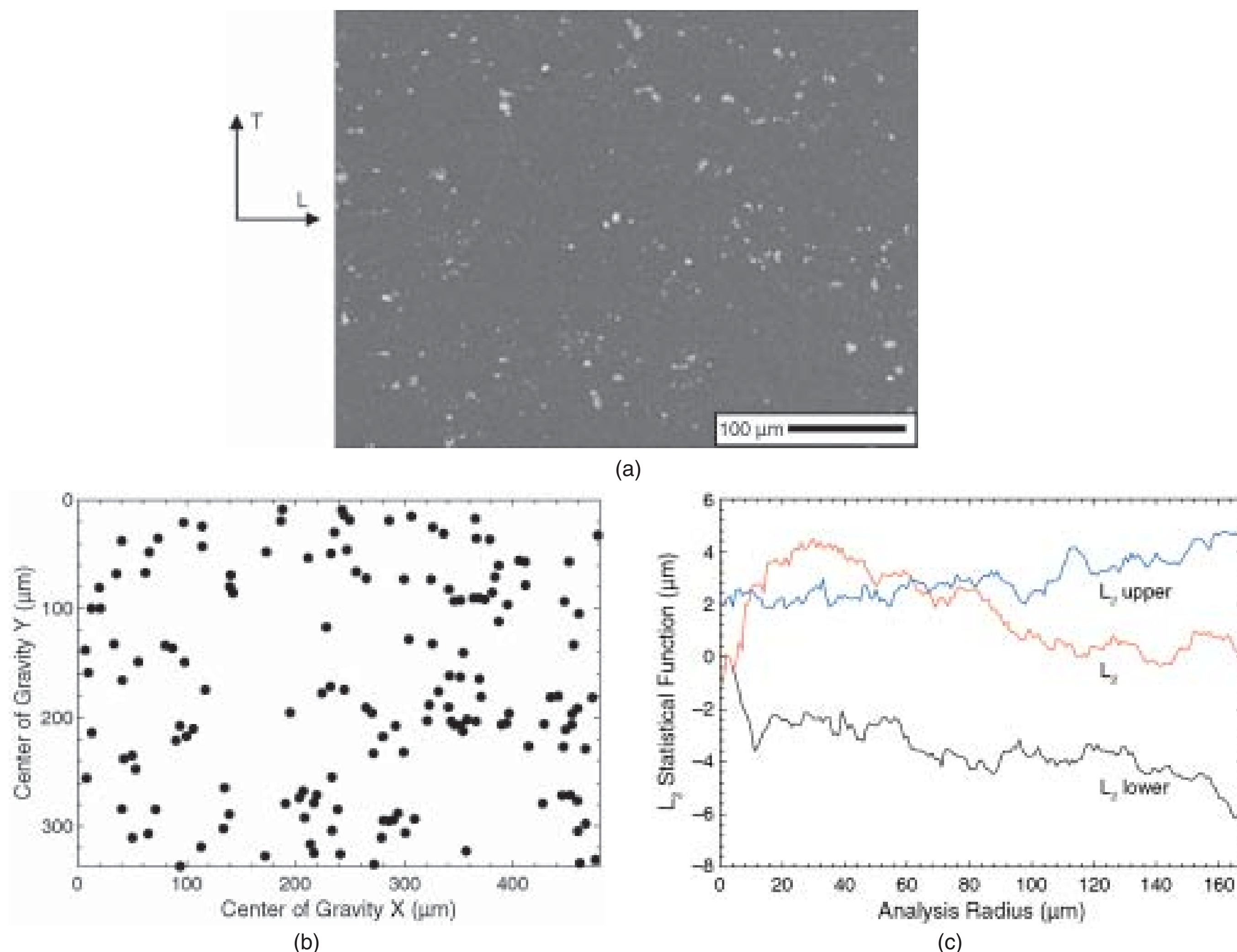

FIGURE 2. *L_2 statistical point pattern spatial analysis of the IMC on the LT surface of AA2024-T3.*

in 80% relative humidity (RH) air chambers at 25°C, 40°C, and 50°C for a period of approximately 75 days. Scribe-creep was monitored in-situ using a digital camera, exploiting the translucent coating to detect the underpaint corrosion front. The rate of scribe-creep was determined and ranked according to scribe-creep susceptibility for the different surface pretreatments. For posttest analysis of these panels, the coating was removed using a tape pull method while the coating was still moist from exposure.

It is important to note why this test was used instead of the ASTM-B117[62] salt spray test. It has been shown that a coating test involving an HCl dip followed by testing in 85% RH humid air at 40°C correlated the best with seacoast exposures at the Pt. Judith, Rhode Island, Alcoa Test site from the standpoint of correlation between lab and field scribe-creep results on coated Al-based alloys.[63] The HCl dip test method consistently correlated with the field results on a variety of Al-based alloys while the ASTM-B117 salt spray test results did not.[63] The test was cyclic in nature in that high humidity periods were punctuated by removal to lower humidity and reapplication of HCl.[41,63]

The micrographs taken periodically of scribe-creep length and area were analyzed in a method similar to that of Bautista[31] and Williams and McMurray.[35] Analysis of the collected data included the quantitative determination of the extent of scribe-creep by visual estimation of the average length, l_{ave}, of the filaments:

$$l_{ave} = \frac{l_i}{N} \tag{1}$$

where l_i is the total length of the filaments measured from the original scratch and N is the number of filaments measured. The delaminated area, $A_{scribe\text{-}creep}$, due to the scribe-creep, calculated using Equation (2), was also estimated:

$$A_{scribe-creep} = A_{corroded} - A_{scribe} \tag{2}$$

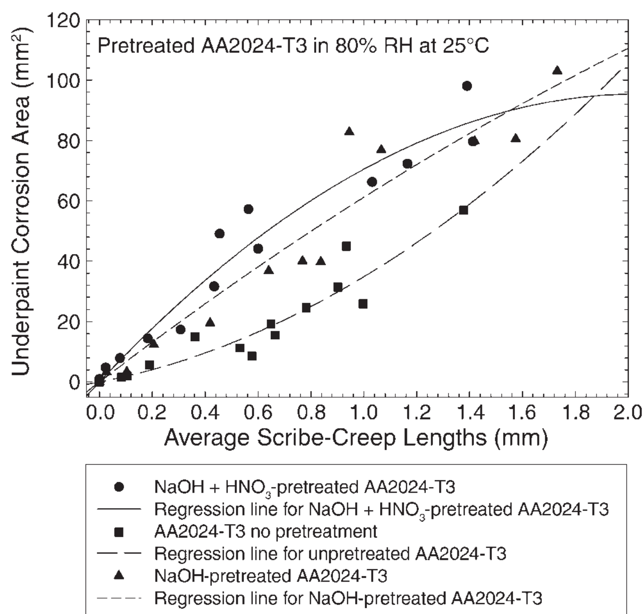

FIGURE 3. *Correlation of the scribe-creep area with the average scribe-creep length for various pretreatments on AA2024-T3 exposed in 80% RH at 25°C.*

Figure 3 shows that the scribe-creep area correlates well with the average scribe-creep length. This indicates that average length can be used to characterize the scribe-creep growth behavior. Posttest analysis on the humidity test panels, after removal of the coating, included the cyclic voltammetric scans as was discussed earlier to determine any global increase in the surface Cu content after the humidity exposure tests. This test was performed after 1 min ultrasonic cleaning in 18.2 MΩ ultra pure water to remove the loose corrosion product with minimal possible Cu removal.

SEM was also performed on these panels to determine the morphology of the underpaint corrosion damage from the scribe creep. Prior to using the SEM, the samples were cleaned to remove the corrosion product from the surface. To clean the panels, without introducing additional corrosion damage, concentrated (15.8 M) HNO_3 was used for approximately 10 min in an ultrasonic cleaner. This cleaning procedure was found to minimize additional corrosion damage.[64]

RESULTS

Effect of Pretreatment on Surface Cu

The pretreatments and preexposures performed on AA2024-T3 affected the extent of Cu replating. Cyclic voltammetry for determining the Cu surface coverage relied on the Cu oxidation reaction peaks and peak areas as shown in Figure 4.[(4)] The peaks appearing at about –0.1 V_{SCE} and between 0 and 0.1 V_{SCE} are the $Cu^0 \rightarrow Cu^I$ and $Cu^I \rightarrow Cu^{II}$ oxidation peaks, respectively. The first peak, which corresponds to the $Cu^0 \rightarrow Cu^I$ oxidation reaction, was more pronounced. Good correlation between peak height (e.g., peak current) and area (e.g., peak charge) was obtained (Figure 5).[60-61] Hereafter peak height was used given its equivalence. When qualitatively comparing the three pretreatments used for this study (Figure 4), it is evident that more Cu was deposited on the surface of the NaOH alkaline-etched sample compared with either the samples with no pretreatment or those with the NaOH + HNO_3 pretreatment. The latter two appear to be fairly similar in the amount of Cu replated on the surface with a slightly greater concentration after the NaOH + HNO_3 pretreatment than in the as-received state. Figure 4 shows that the NaOH + HNO_3 pretreatment cleaned the surface of replated Cu produced by NaOH exposure. Moreover, it may also have eliminated some of the future sources of Cu, such as the smaller Al-Cu-Mg-type particles and therefore decreased the capacity of Cu available for replating. However, the larger particles of that composition remained on the surface and a source of Cu was available for replating during scribe-creep.[2,56]

Bare, unpretreated and NaOH + HNO_3-pretreated AA2024-T3 samples were also exposed to a variety of other solutions to examine the propensity for Cu replating in solutions crudely simulating head or tail solutions under FFC tracks. These included neutral 0.05 M sodium chloride (NaCl) in lab air as well as simulated head/tail solutions (i.e., 0.5 M NaCl, pH = 4, at 40°C and 0.05 M NaCl, pH = 10, at 40°C, respectively). During the corrosion process in NaCl, additional Cu was replated on the surface in the case of both pretreatments. Figure 6(a) shows the relative values of the Cu peak heights after the various exposure times in near-neutral 0.05 M NaCl. The peak height obtained on pure Cu is also plotted for comparison. The Cu peak height for the unpretreated AA2024-T3 coupons increased with exposure time in neutral 0.05 M NaCl solution. A dramatic increase in the Cu peak height occurred during the first 10 h of exposure and then a slow gradual increase was observed with additional exposure time. However, much less Cu replating was detected than for the full monolayer coverage present on pure Cu. The initial concentration was greater for the NaOH + HNO_3-pretreated samples exposed to 0.05 M NaCl, and the maximum Cu peak height occurred after about 10 h. Then the peak height decreased slightly with increasing exposure time. Figure 6(a) also shows that a large amount of Cu was replated onto the surface during even short NaOH exposures times (this effect of exposure time in 1.5 g/L NaOH can be seen more easily in Figure 6[b]). The amount of Cu replated on AA2024-T3 in 1.5 g/L NaOH was greater than the amount replated during the long exposures in 0.05 M NaCl. Figure 6(c) illustrates that more Cu was replated on the unpretreated

[(4)] Both Cu-containing IMC and replated Cu have been confirmed to exhibit Cu oxidation peaks.

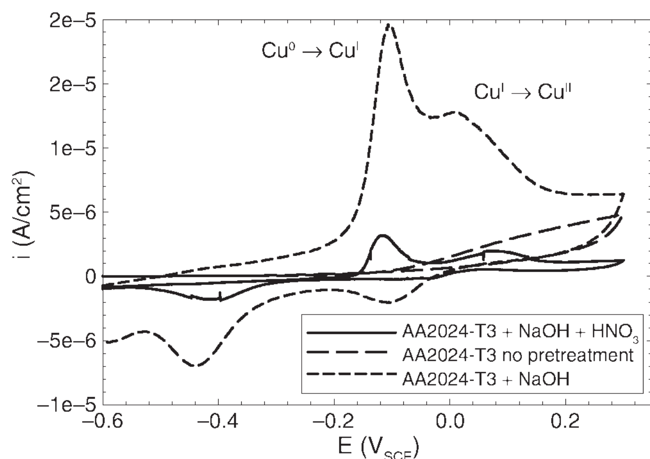

FIGURE 4. *Cyclic voltammetry of Cu oxidation and reduction reactions in deaerated borate buffer (pH = 8.4) on 40 min NaOH pretreated, unpretreated, and 40 min NaOH + 30 s. HNO_3-pretreated AA2024-T3.*

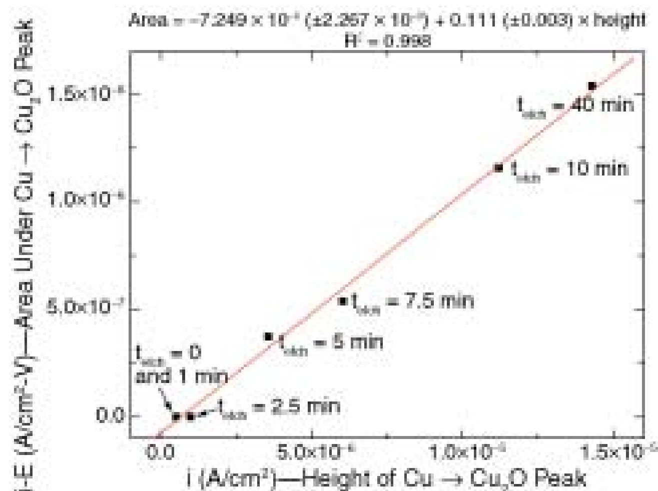

FIGURE 5. *Linear correlation of Cu oxidation peak area against Cu oxidation peak height from NaOH-treated AA2024-T3 at the indicated etch times.*

AA2024-T3 exposed in the 0.05-M NaCl solution at pH = 10 than on the unpretreated AA2024-T3 in the 0.5-M NaCl solution at pH = 4 or on the NaOH + HNO_3-pretreated AA2024-T3 exposed in either high- or low-pH solutions at 40°C. This effect is more obvious in Figure 6(d), which shows the change in Cu peak height, $i-i_o$, where i_o is the initial Cu peak height at zero exposure. Figures 6(a) and (c) imply that the tail of a filiform would have a higher capacity for Cu replating in the unpretreated case at 40°C than in the NaOH + HNO_3-pretreated case at 40°C. Figures 6(a) and (b) show that after a 20-min exposure in the NaOH solution a maximum peak height was reached, in which the peak height was roughly equivalent to that measured on pure Cu. Therefore, it was reasonable to assume that the NaOH pretreatment yields more surface Cu than any other treatment performed. After a 20-min exposure of unpretreated AA2024-T3 to 1.5 g/L NaOH solution, the height of the cyclic voltammetric peaks no longer increased, suggesting that little additional Cu could be replated or exposed on the surface after the 20-min exposure in this alkaline solution. The results shown in Figures 6(a) through (d) imply that the initial amount of replated Cu as well as the capacity to replate Cu depends on the pretreatment and exposure conditions.

SEM performed before and after NaOH + HNO_3 pretreatment showed that after pretreatment many IMC were still present on the surface, including the larger S-phase constituent particles (Figure 7). Recall that both the unpretreated and NaOH + HNO_3-pretreated samples were exposed to a neutral 0.05-M NaCl solution for up to 122 h (Figure 6[a]). The Cu peak heights for each condition were approximately equal. This result is reasonable, since the presence of constituent particle fragments act as Cu sources for replating.

Cathodic polarization scans performed on pure Cu, pure Al, unpretreated AA2024-T3, NaOH-pretreated AA2024-T3, and NaOH + HNO_3-pretreated AA2024-T3 are shown in Figure 8. A comparison of pure Cu, AA2024-T3, and pure Al indicates how significantly the oxygen reduction reaction (ORR) depends on Cu content (Figure 8[a]). A large increase in the net cathodic reaction rate in the mixed charge transfer/mass-transfer regime was observed over the range in potential from –0.3 V_{SCE} to –0.7 V_{SCE}. Moreover, the mass-transport-limited current density increased from pure Al to the unpretreated AA2024-T3 to the pure Cu. The limiting current density increased toward values measured on pure Cu with an increased alkaline etch time. Thus, replated Cu should enhance the ability to support underpaint corrosion on Al by enhancing the cathodic ORR rate in the scribe-creep wake as well as in the scratch area.

Morphology of Underpaint Corrosion Associated with Scribe-Creep

Scribe-creep exposures on the pretreated, coated, and scribed AA2024-T3 as well as Al were conducted for ~75 days at 25°C, 40°C, and 50°C in 80% RH using lab air. Figure 9 illustrates the scribe-creep that was observed. Figure 9 also shows that the scribe-creep damage grew in the L direction from the induced defect in the coating (scribe) and grew in both L directions away from the scribe.

SEM was performed on the NaOH pretreated, unpretreated, and NaOH + HNO_3-pretreated and coated panels after scribe-creep testing in humid air and coating removal. The surface morphology for each pretreat condition after exposure to 80% RH at 40°C for ~75 days is shown in Figure 9. The surface morphologies of the three pretreatments were similar. The main

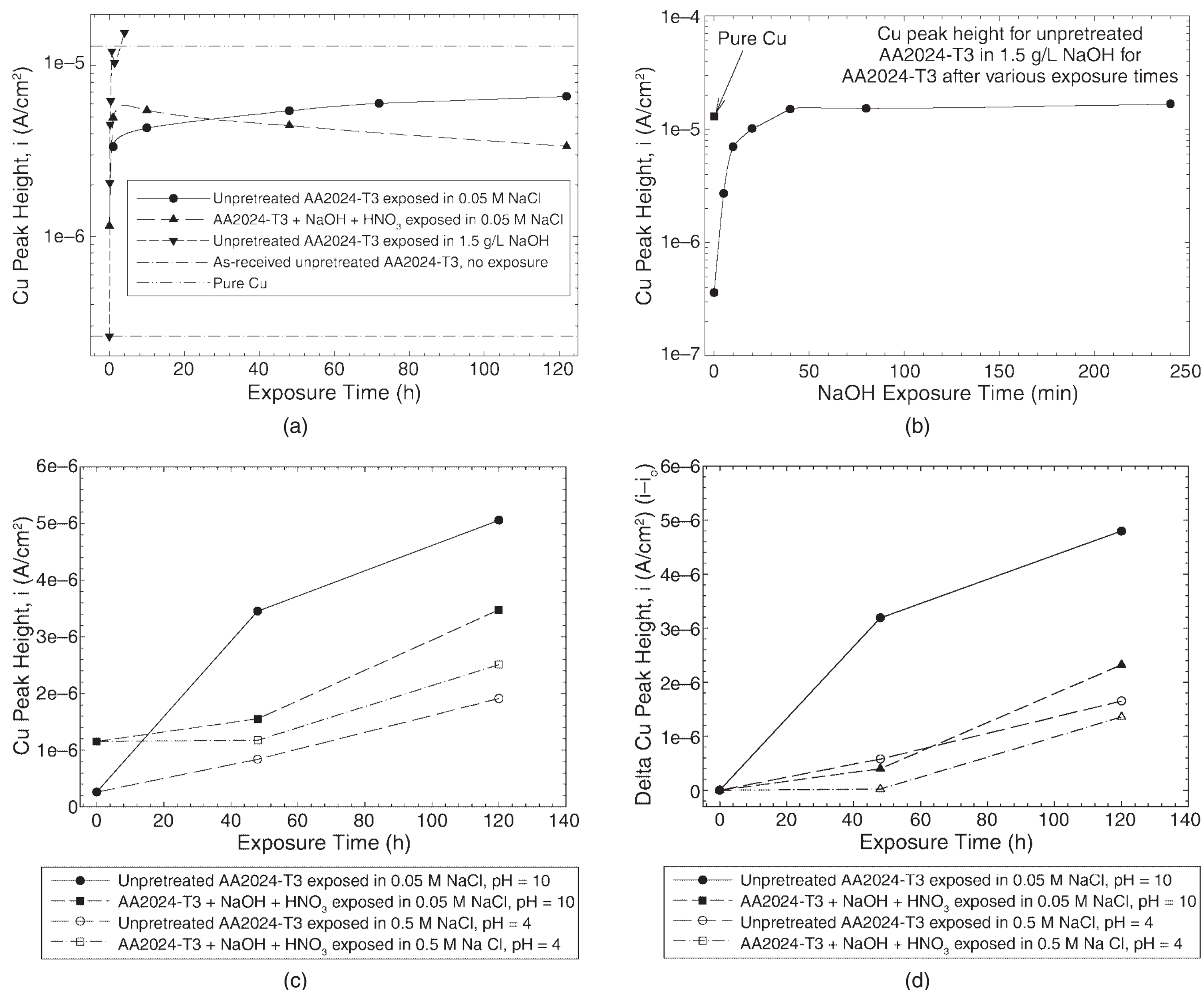

FIGURE 6. *The Cu peak heights from cyclic voltammograms on pretreated and unpretreated AA2024-T3 in deaerated borate buffer (pH = 8.4): (a) after no exposure, as well as exposures to room temperature NaCl and NaOH for various time periods. The effect of short 1.5-g/L NaOH exposure times is more clearly shown in (b). The peak height for pure Cu is shown for comparison purposes. (c) The Cu peak heights after exposure in the simulated tail solution (0.05 M NaCl, pH = 10) and simulated head solution (0.5 M NaCl, pH = 4) at 40°C for various exposure times. The change in Cu peak heights from the exposure in the simulated tail and head solutions is shown in (d).*

difference was the amount (i.e., length and area [to be shown below]) of overall scribe-creep as well as the width of the filaments. The filaments on the NaOH-pretreated sample grew together to form a large, dense corroded area. The unpretreated sample showed a similar surface condition, but distinct filaments were still visible. The scribe-creep filaments on the NaOH + HNO_3-pretreated sample were more scattered and consisted of distinct, separate filaments that did not grow very long in the time period of the humid air exposure. Figure 9(a) shows an overall image of the scribe-creep area for the NaOH-pretreated sample as well as high-magnification views of specific regions. The surface in the wake of the scribe-creep track had large pits present with an intergranular appearance, suggesting an acidic environment was present.[5] The area just in front of the head of a filament showed some etching, trenching, pitting, and possible intergranular attack. The micrograph taken at a distance away the scribe-creep where the coating was not damaged shows the damage from the pretreatment process independent of scribe-creep. Pretreatment mainly attacked constituent particles in addition to Cu-replating as discussed

[5] It is well known that acidic oxidizing chloride environments attack precipitation age-hardened Al alloys and can cause intergranular corrosion, if susceptible. An example of this is the ASTM G-110 test environment where acidified sodium chloride + hydrogen peroxide solution is used to test for intergranular corrosion susceptibility.

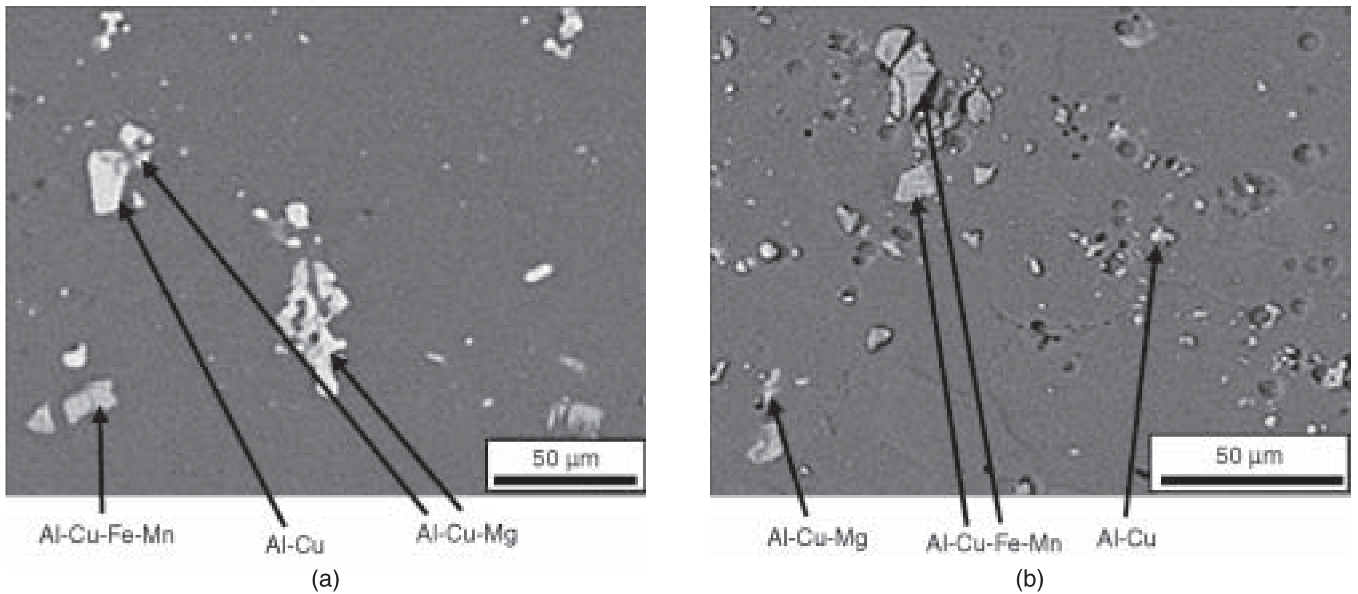

FIGURE 7. *Scanning electron micrographs of LT surface of AA2024-T3 showing the Al-Cu, Al-Cu-Mg, and Al-Cu-Fe-Mn-type constituent particles on the: (a) unpretreated and (b) NaOH + HNO_3-pretreated surfaces.*

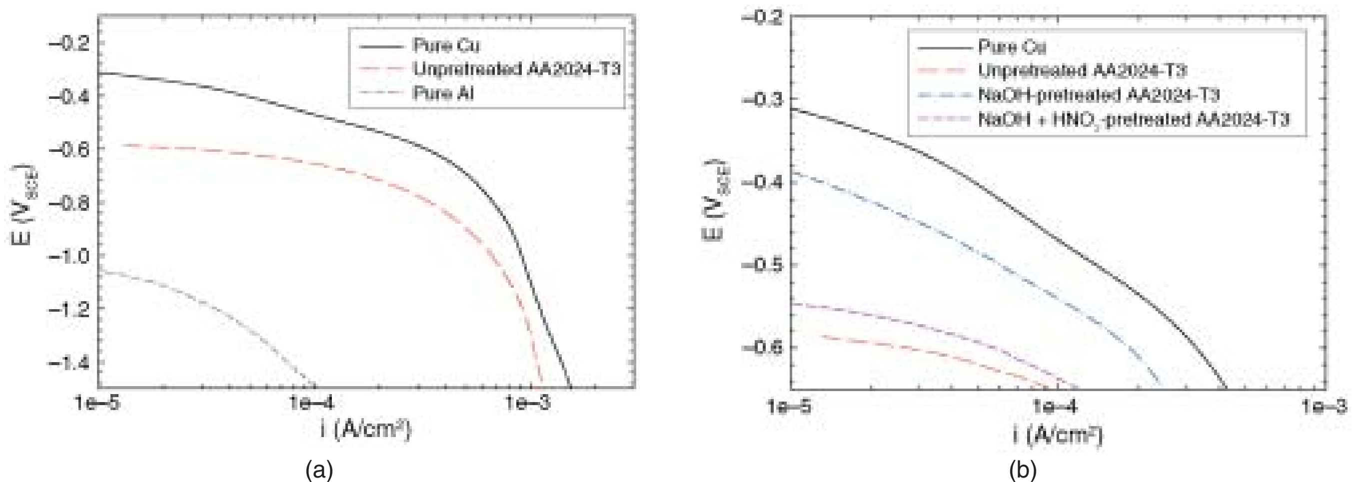

FIGURE 8. *Cathodic potentiodynamic polarization scans on rotating disk electrodes in pH = 8.2 borate buffer at a rotation rate of 1,500 rpm: (a) cathodic scans for pure Cu, unpretreated AA2024-T3, and pure Al and (b) enlarged cathodic charge-transfer region for pure Cu, unpretreated AA2024-T3, NaOH-pretreated AA2024-T3, and NaOH + HNO_3-pretreated AA2024-T3.*

above. Significant localized corrosion damage (pitting and some intergranular attack) in all three cases occurred in the wake of the scribe-creep track. Both the unpretreated and NaOH + HNO_3 samples showed similar surface morphology at the front of the filament head, as was observed on the coated NaOH pretreated sample (Figures 9[b] and [c]). Pits and intergranular corrosion were also observed in scribe-creep areas. As with the NaOH-pretreated sample, the NaOH + HNO_3 sample showed localized constituent particle damage far away from the scribe-creep, indicating that both pretreatments preferentially attacked the constituent particles on the surface of the AA2024-T3.

Effect of Temperature, Alloy, and Pretreatment on Scribe-Creep Rate

Scribe-creep experiments on pure Al showed that little underpaint corrosion occurred over the experimental time period. However, an increase in underpaint corrosion occurred with the addition of Cu and Mg to the Al in the form of AA2024-T3, as shown in Figure 10. The scribe-creep data shown in this plot indicate that there was no incubation time associated with the scribe-creep, or that the incubation time was shorter than the data collection frequency. The length of scribe-creep observed on the unpretreated AA2024-T3 panel (Figure 10) increased more slowly with longer times, indicating that the

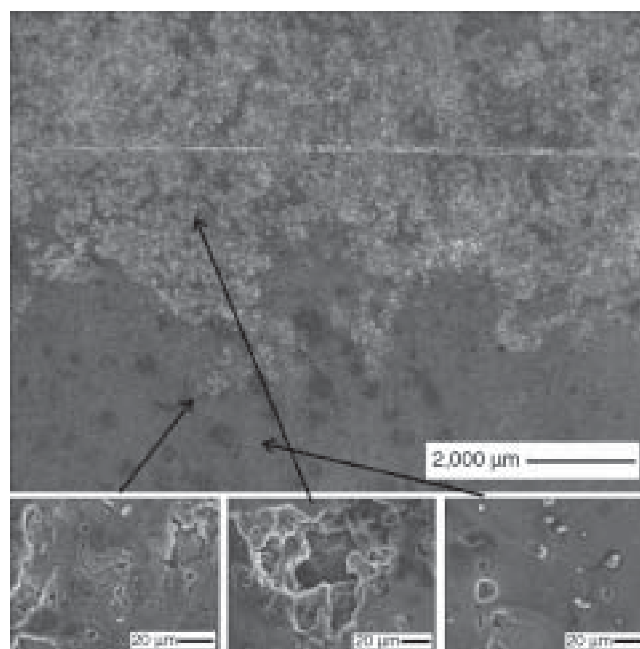

(a)

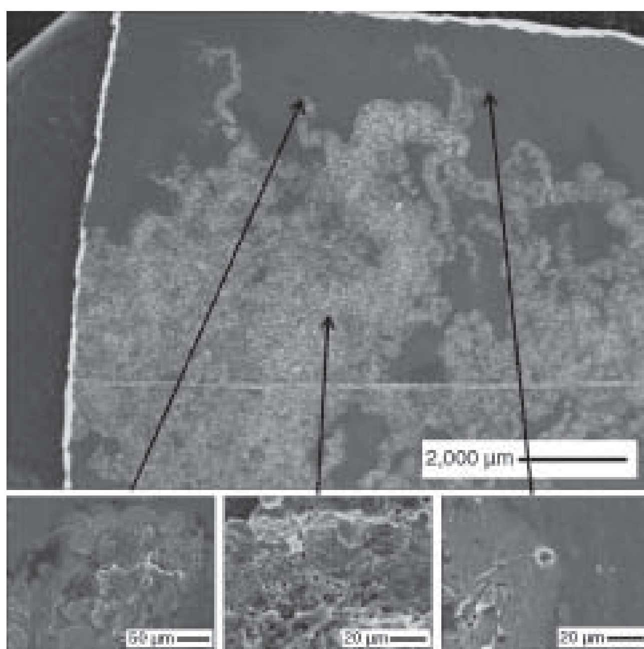

(b)

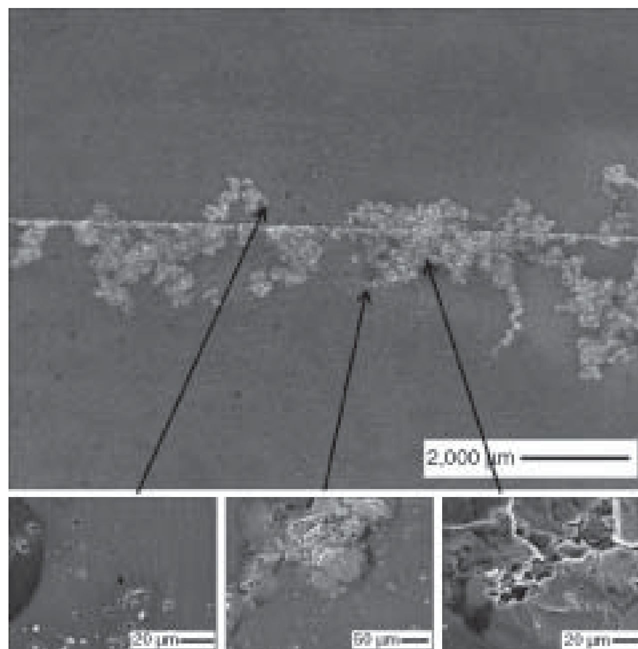

(c)

FIGURE 9. *Scanning electron micrographs on AA2024-T3: (a) NaOH pretreatment, (b) no pretreatment, and (c) NaOH + HNO_3 pretreatment after scribe-creep in moist air at 80% RH and 40°C. Micrographs were taken after organic coating removal and specimen cleaning. The arrows indicate the locations of the enlargement micrographs that were taken in the wake of the scribe-creep area, just in front of the head of a filament, and in the case of the NaOH-pretreated panel far away from the underpaint corrosion.*

growth rate decreased slowly over the period of the exposure.

Increasing the exposure temperature resulted in an increase in scribe-creep growth rates and overall average scribe-creep lengths for unpretreated AA2024-T3 after a fixed period. This increase is observed in Figure 11 for the unpretreated AA2024-T3. There was still a decrease in the growth rates over the exposure period at all temperatures, as shown in Figure 12. The largest increase in the scribe-creep growth rate was observed when the exposure temperature was elevated to 50°C. Figure 12 shows that

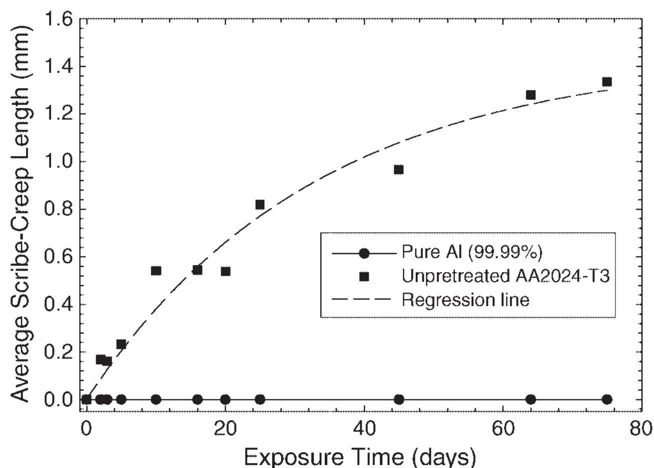

FIGURE 10. *Effect of alloying on the scribe-creep growth on unpretreated AA2024-T3 in 80% RH at 25°C. The length of scribe-creep as a function of exposure time.*

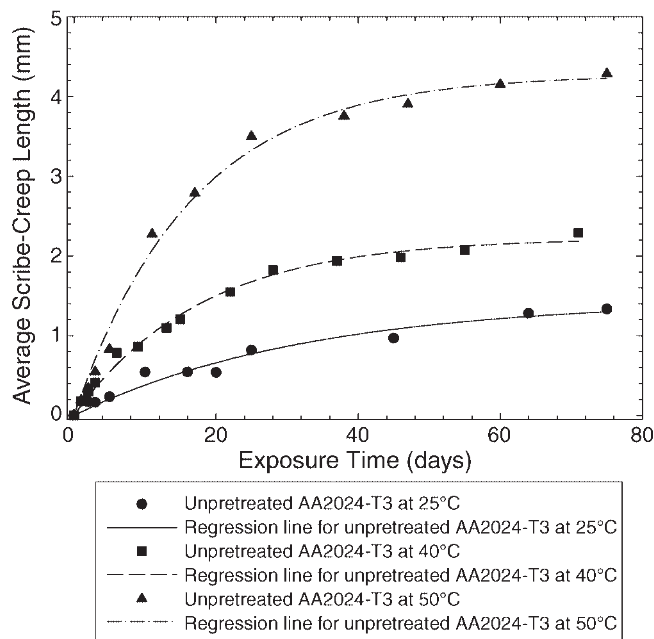

FIGURE 11. *Effect of increasing temperature on the scribe-creep lengths for unpretreated AA2024-T3 in 80% RH at 25°C, 40°C, and 50°C.*

at higher temperatures there also did not appear to be an incubation period for the underpaint corrosion on the unpretreated AA2024-T3 panels. If the average scribe-creep length is plotted as a function of $t^{1/2}$, a roughly linear relationship is found (i.e., $l \propto t^{1/2}$), Figure 13. Assuming $t^{1/2}$ behavior, curves can be used to calculate the activation energy for each temperature utilizing Equations (3) and (4). Equation (3) shows time dependence and contains a constant, which includes a thermal activation term:

$$\frac{dl_{ave}}{dt} = \frac{kt^{-1/2}}{2} \tag{3}$$

$$k = k_o \exp^{\left(-Ea/RT\right)} \tag{4}$$

The integral of Equation (3) can be used to fit the measured data (Figure 13), showing that the scribe-creep growth rate increases with exposure temperature according to a simple Arrhenius expression.[6]

The humidity exposure temperature affected both the unpretreated as well as the pretreated panels. It was observed that the scribe-creep growth rate on the NaOH-pretreated panels also increased with temperature. Figure 14 shows the scribe-creep growth length over time as a function of the temperature. The growth rate decreased over the exposure period at all temperatures for NaOH-pretreated AA2024-T3. At the end of the test period, the growth rates for all three temperatures were roughly the same but the average

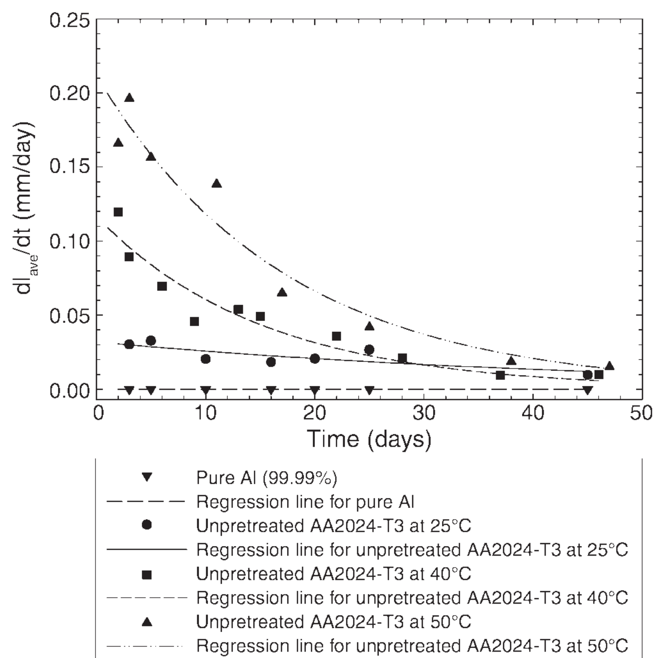

FIGURE 12. *The effect of increasing temperature on the scribe-creep growth rate for unpretreated AA2024-T3 in 80% RH at 25°C, 40°C, and 50°C.*

length of scribe-creep at each temperature differed because of the effect of temperature in the early stages of exposure.

In case of the NaOH + HNO_3-pretreated panels the scribe-creep length was not increased by increas-

[6] The data for the various pretreatments did not provide a perfect fit to the linear l vs. $t^{1/2}$ curves at all temperatures at all times. Thus, it should be noted that k-values for all conditions may only apply over a restricted portion of time. Hence, the n values may not be uniquely equal 1/2 over the entire exposure time. This could be explained by a change occurring in the growth rate mechanism for scribe-creep over the exposure period. Possibly a change in the dominant controlling factor during galvanic corrosion occurred over the exposure time.

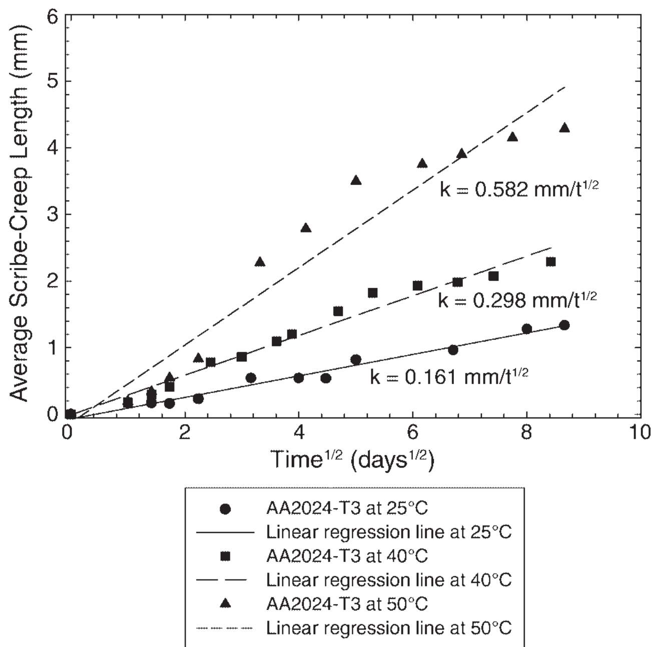

FIGURE 13. *The average scribe-creep length as a function of $t^{1/2}$, where the slope of the line is equal to k.*

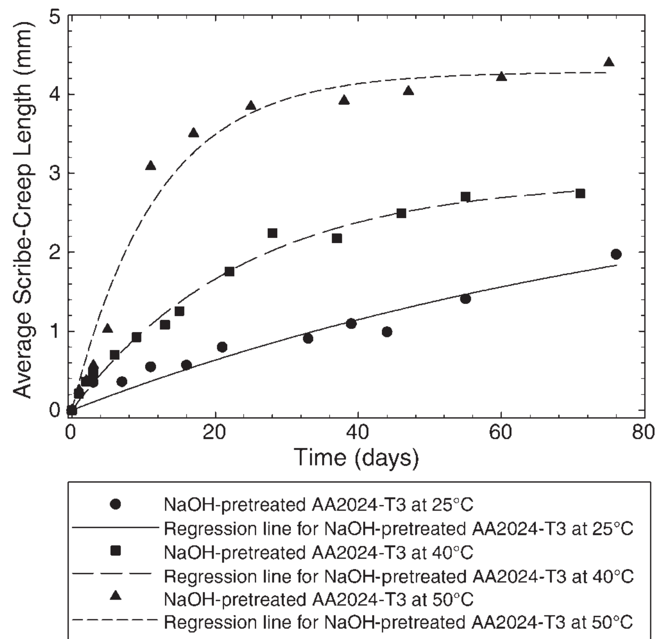

FIGURE 14. *Effect of temperature on the average scribe-creep lengths with exposure time of NaOH-pretreated AA2024-T3 in 80% RH at temperatures of 25°C, 40°C, and 50°C.*

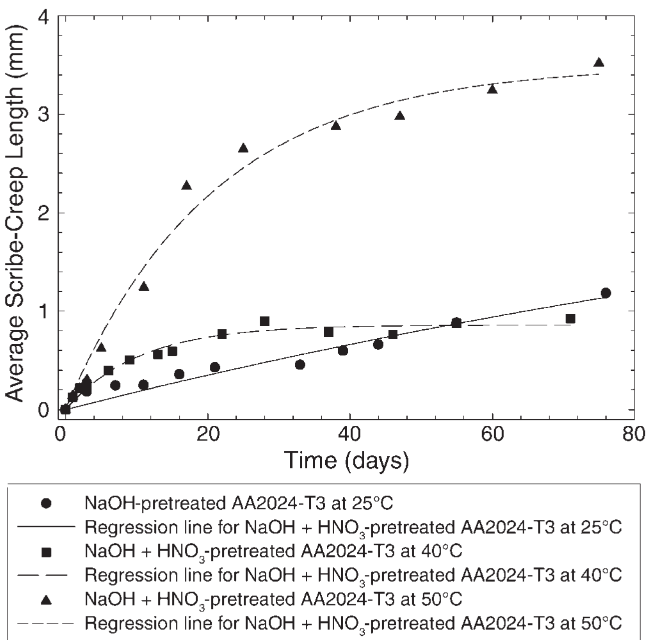

FIGURE 15. *Effect of temperature on the average scribe-creep lengths with exposure time of NaOH + HNO_3-pretreated AA2024-T3 in 80% RH at temperatures of 25°C, 40°C, and 50°C.*

ing the temperature from 25°C to 40°C (Figure 15). However, when the temperature was increased to 50°C, a large increase in the length was observed at early times. The scribe-creep growth rate of the NaOH + HNO_3-pretreated panels was higher at 50°C. However, the scribe-creep rate at 50°C decreased to rates observed for 25°C and 40°C at the end of the test period. At 25°C, the growth rates of the unpretreated and NaOH + HNO_3-pretreated panels were approximately the same and much lower than the growth rate of the NaOH-pretreated panels. At 40°C, the scribe-creep growth rates of the NaOH-pretreated and unpretreated panels were much higher than those on the NaOH + HNO_3-pretreated panels, although at the conclusion of the test period all the rates were approximately the same. At 50°C, the scribe-creep growth rate was high for all three pretreatments, but the initial rate for the NaOH + HNO_3 pretreatment was still lower than the grow rates on the NaOH-pretreated and unpretreated panels. As in the case of the growth rates at 25°C and 40°C, the scribe-creep growth rates were considerably slower at the end of the exposure time for 50°C, regardless of pretreatment. To summarize, temperature-accelerated scribe-creep rates and scribe-creep rates slowed with time for all pretreatments. Temperature had the most pronounced effects for NaOH-pretreated specimens.

If we assume that n has a value of ½ for the NaOH-pretreated and NaOH + HNO_3-pretreated panels, as was done in the unpretreated case shown in Figure 13, a slope or k-value can be determined. To determine the activation energy for the scribe-creep process, the k-values were determined as shown earlier in Figure 13. The natural logarithms of these k- values were then plotted as a function of T^{-1} (K), as shown in Figure 16. The linear regression line for each pretreatment was assumed to take the following form:

$$\ln k = \ln k_o - \left(\frac{E_a}{R}\right)\frac{1}{T} \quad (5)$$

where ln k_o is the y intercept, E_a is activation energy, and R = 8.314 J/mol·K. The fitted lines are shown in Figure 16 along with the experimental data points and the values are reported in Table 1. It was not possible to determine an activation energy for the case of the NaOH + HNO_3-pretreated AA2024-T3 due to the scatter in the data. However, it is clear that the k-values after this pretreatment were lower at each temperature. In fact, the following trend was observed at each temperature:

$$k_{NaOH} > k_{unpretreated} > k_{NaOH+HNO3} \quad (6)$$

Assay of Copper Contents on Scribe-Creep Surfaces

Cyclic voltammetry tests were performed on scribe-creep samples for the unpretreated, NaOH-pretreated, and NaOH + HNO_3-pretreated samples prior to coating and exposure to 80% RH at 25°C, 40°C, and 50°C. Figure 17 shows that the scribe-creep length after ~75 days' exposure was greatest for the NaOH-pretreated samples, which had the largest initial Cu peak height on the cyclic voltammetric scans prior to organic coating deposition and any exposure. The unpretreated samples had a similar Cu peak height compared to the NaOH + HNO_3-pretreated samples, but had the larger average scribe-creep length. This could be explained by the greater capacity for Cu replating during exposure as suggested by Figures 6(c) and (d). Note that differences are small at 25°C and the amount of Cu replated was similar for unpretreated and NaOH + HNO_3-pretreated cases. According to Figure 17, temperature significantly affected the scribe-creep results at any given Cu coverage.

Cyclic voltammetric tests were also performed on the post-humidity exposure scribe-creep samples in the case of the unpretreated, NaOH-pretreated, and NaOH + HNO_3-pretreated samples tested in 80% RH

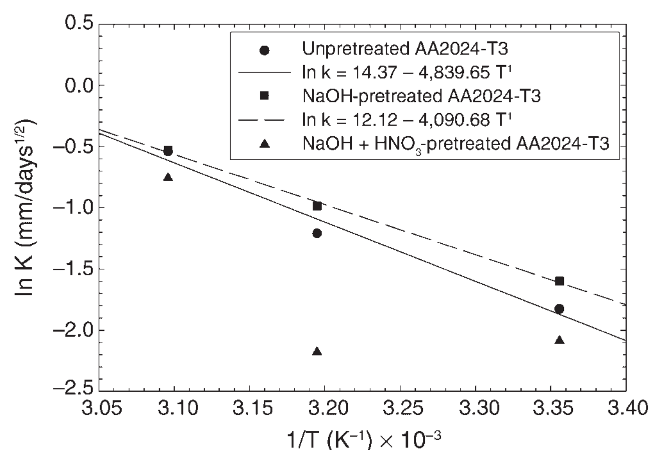

FIGURE 16. *Arrhenius plots derived from scribe-creep data for the NaOH + HNO_3-pretreated, unpretreated, and NaOH-pretreated conditions.*

at 25°C and 40°C. The test area for the cyclic voltammetric scans was an overall specimen area, which contained both scribe-creep and uncorroded area. Therefore, an increase in Cu peak height was indicative of a larger area upon which Cu had been replated as well as a larger amount of Cu per unit area. The resultant Cu peak heights were plotted against the measured scribe-creep length for all pretreatments at the two temperatures (Figure 18). The scribe-creep length increased nonlinearly as the Cu peak height increased. For the Cu assay conducted after exposure, the Cu peak height for the unpretreated case surpassed the NaOH + HNO_3-pretreated case, substantiating the claim that the unpretreated case had a greater capacity for Cu replating. Moreover, for a given Cu peak height, the scribe-creep length was greater as the temperature was raised from 25°C to 40°C. The Cu peak height and the scribe-creep length were lowest for the NaOH + HNO_3-pretreated samples and highest for the NaOH-pretreated samples at each temperature, indicating prior Cu levels as well as additional capacity for replating Cu.

TABLE 1

Parameters k, k_o, and E_a for Thermally Activated Scribe-Creep after the Pretreatments Indicated[A]

Pretreatment	T (K)	k (mm/days$^{1/2}$)	k_o (mm/days$^{1/2}$)	E_a (kJ/mol)
Unpretreated	298	0.161	1.74×10^6	~40.24
	313	0.298		
	323	0.582		
NaOH	298	0.202	1.84×10^5	~34.02
	313	0.373		
	323	0.589		
NaOH + HNO_3	298	0.124	—[B]	—[B]
	313	0.113		
	323	0.469		

[A] $l = kt^{1/2}$ behavior was assumed in all cases.
[B] Values were not calculated due to data scatter.

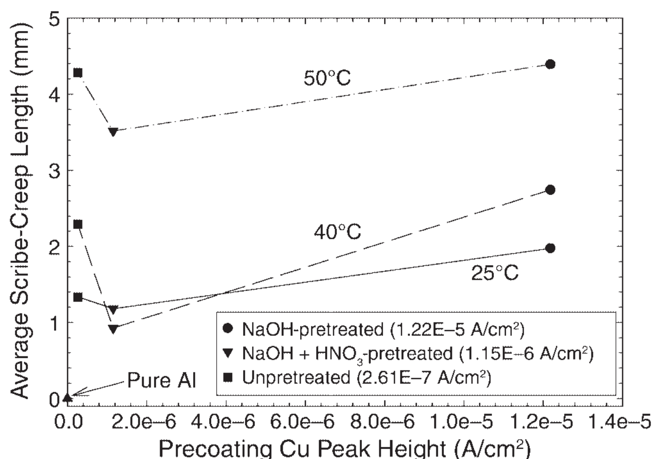

FIGURE 17. *CV peak height prior to coating application as a function of the average scribe-creep length after ~75 days for unpretreated and pretreated AA2024-T3 in 80% RH at 25°C, 40°C, and 50°C.*

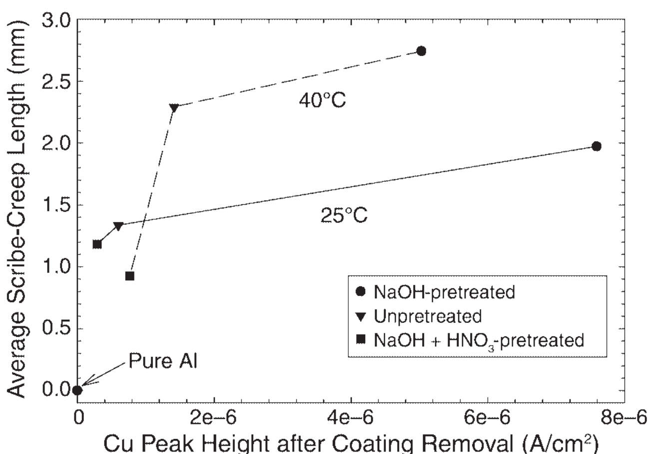

FIGURE 18. *The average scribe-creep length after ~75 days for AA2024-T3 in 80% RH at 25°C and 40°C as a function of Cu peak height after removing the coating.*

DISCUSSION

It is well known that FFC is a form of underpaint corrosion that grows on metal surfaces, underneath a coating, in a thread-like manner.[23,31-41,43-44,47,50,57-59,63,65-78] The filament has what is considered an anodic head and a cathodic tail. The head has an acidified, high Cl^- ion-containing electrolyte present, while the tail consists of semi-dry corrosion product and the pH is alkaline.[35,37,79] The local anode in the leading part of the head of the filament is where the anodic dissolution of the metal occurs and undercuts the coating. Farther back from the leading edge is the local cathode where ETR, such as reduction of oxygen, occurs. The anodic propagation of the filaments has been ascribed to the differential in the oxygen concentration between the front and the back of the head of the filament,[23,31,79] although, clearly, the pH change and Cl^- levels also contribute to the formation of a galvanic couple between the low-pH, high-Cl^- head and high-pH tail. The FFC rate is promoted by HCl solution[35,75] and elevated temperature.[31,43,75,80] Hoch[43] observed that in cold weather, FFC appeared to become inactive and then reinitiated when exposed to warm weather. These findings are all consistent with the present study where the local corrosion morphology under filiform sites (Figure 9) suggests an acidified, high-Cl^- anodic head, where attack is promoted by HCl-containing solution, as expected in the case of pitting and intergranular attack. Recall that pitting and intergranular attack were seen in Figures 9(a) through (c) in the filiform tracks.

Given the galvanic couple between the head and tail, the scribe-creep growth processes that could control galvanic corrosion are diffusion, ohmic, anode, or cathode control, or any combination of these. The primary controlling mechanism can also change over exposure time. If anodic undercutting promotes scribe-creep in Al-based alloys, then the rate of scribe-creep would be directly proportional to the rate of galvanic corrosion and mediated by the state of adhesion. Anodic control is more than likely not one of the controlling mechanisms due to the correlation and interdependency between replated Cu, ORR rate, and scribe-creep growth rate.[(7)] The question is how pretreatment and alloying content affect this galvanic corrosion process. Clearly, Cu content is important, as indicated in Figure 10. Cu replating, in the case of AA2024-T3, is directly related to the reservoir of Cu present at Cu-rich IMC and Cu in solid solution. These compounds can act as local cathodes and a source for Cu that can be replated. It is speculated that enhanced Cu replating increases the driving force for galvanic corrosion and supports cathodic ETR to support the rate of galvanic corrosion, as shown in Figure 8. It is also speculated that scribe-creep is controlled by a charge transfer or mixed charge-transfer/diffusion-controlled ORR as well as the ohmic resistance between the head and tail. As this ohmic resistance increases, the galvanic corrosion process may slow down. This will be the subject for a future publication. However, it stands to reason that an increase in the amount of available Cu on the surface increased the rate of the charge transfer and diffusion-controlled reduction of oxygen reaction (Figure 8[b]). This correlates with an increase in the growth rate of the FFC, which was observed from the scribe-creep test data (Figures 11 and 14) when the increase of surface Cu was promoted using an alkaline etch.

The scribe-creep tests showed that Cu was necessary in order for scribe-creep to occur, and it was verified by its absence on pure Al (99.99%) in Figure 10. It was also observed from Figures 11, 14, and 15

[(7)] Anode control may play a role in altered microstructures that produce faster anodic reaction rates such as Cu-depleted overaged alloys.

that the AA2024-T3 panel with the highest amount of surface Cu (NaOH-pretreated) exhibited the highest average scribe-creep length and growth rate. The AA2024-T3 surface with a low-Cu content (e.g., AA2024-T3 after 40 min in NaOH and 30 s in HNO_3 pretreatment), where the Cu on the surface as well as from most of the IMC was removed by the HNO_3 treatment, exhibited the lowest amount of scribe-creep. Obviously not all of the Cu available for replating and subsequent oxygen reduction was removed during the HNO_3 exposure; otherwise, the scribe-creep growth rate for this pretreated condition would have been similar to that of pure Al. Moreover, the original scribe area penetrated beneath the pretreated surface, exposing new sources of Cu. Figure 7 clearly showed that constituent particles are still present on the surface after the NaOH + HNO_3 pretreatment. One source of Cu for replating is the IMC, particularly S-phase. Recall that S-phase (Al_2CuMg) is anodic to the Al alloy matrix.[2-3,12,15,17-18] Small Al_2CuMg IMC should easily dissolve to release more Cu in the filament wake to support scribe-creep.[2-3,12,15,17-18]

Increasing the scribe-creep temperature to 40°C was found to have the largest effect on the scribe-creep length and growth rate of the AA2024-T3 sample with no pretreatment. One reason for this finding could be that there was a larger capacity of Cu available to be replated than in case of the HNO_3-pretreated sample (Figures 6[c] and [d]), which is seen in the high-pH solution simulating the scribe-creep tail.

The linearity of the Arrhenius plots suggests that the scribe-creep growth process follows a simple Arrhenius process. The activation energies are fairly similar for all the pretreatments, ranging between 34 kJ/mol and 41 kJ/mol. However, the values for k_o are different for each pretreatment. This activation energy also supports the notion that the rate is controlled by ETR instead of oxygen transport in the bulk electrolyte phase or through a polymer because significantly lower activation energies are seen when the latter phenomena are controlling.[81-86] For example, the diffusion of water molecules through a bulk water phase in the polymer (polybutadiene) on steel is about 19.2 kJ/mol.[85] Ruggeri and Beck[34] calculated that the rate of diffusion through the tail was ten times that needed to support corrosion and more than ten times greater than the diffusion rate through many of the polymer coatings, which was supported by the observation of FFC, even when an O_2 impermeable metallic coating was used. The activation energy for O_2 transport in an aqueous phase is quite low, changing only 1% to 2% per °C.[87] Moreover, Leidheiser, et al.,[83] calculated activation energies of 45.2 kJ/mol to 56.5 kJ/mol for various chloride-containing electrolytes from delamination rates of polybutadiene coating on steel, which proceeds by an entirely different mechanism that relies on cathodic disbondment. The cathodic disbondment of steel relies on OH^- production, which, in turn, relies on the rate of the oxygen transport and reduction reaction on steel. Barrer[82] measured activation energies of 25.1 kJ/mol to 50.2 kJ/mol for gas permeation through the polybutadiene coating on steel, and Van Amerongen[86] measured activation energies of 28.5 kJ/mol for oxygen diffusion through polybutadiene. These activation energies are somewhat lower than what was observed in this study. Considering the fact that the larger Cu coverage brought about by the alkaline etch results in a higher charge-transfer-controlled oxygen reduction current density (Figure 8), as well as a larger limiting current density for ORR, suggests that the activation energy associated with this ETR process controls the activation energy seen in scribe creep. The increase in temperature could increase the cathodic reaction rates, especially the charge-transfer-controlled rate, which is thermally activated via the effect of temperature on exchange current density at similar activation energies. Indeed, the proton discharge ETR can range from 25 kJ/mol to 70 kJ/mol.[87] Additionally, the increased temperature could also decrease the adhesion of the coating providing another cause for this increase in scribe-creep.

A decrease in the scribe-creep growth rate over time was also observed for each pretreatment at each temperature. If the observed scribe-creep growth is an ohmic-controlled process, the decreasing growth rate would indicate that the ohmic path length increased over the course of the exposure period. A decrease in rate was observed to occur after ~20 days at each temperature and pretreatment. Mol, et al.,[50] proposed that the decrease or stagnation of the filament growth rate as the filament lengthens is due to the accumulation of corrosion product in the tail of the filaments, which entraps chloride. This entrapment of chloride could decrease the ability for chloride to be transported to active head sites in support of the formation of an acidified, low-pH anodic head. It is more likely that ohmic resistance is increased between dominant anodes and cathodes. In this view, the rate of scribe-creep is operating as a galvanic couple that is controlled by the cathodic charge-transfer reaction rate and the ohmic electrolyte resistance between the head (anode) and tail (cathode) that form a galvanic couple. If a large portion of the cathode remains in the scratch or at the wake of the scribe-creep near the scratch, this ohmic resistance increases over time as the active head moves further away. The galvanic corrosion rate must then decrease with scribe-creep length for the same galvanic driving force. A decrease in galvanic corrosion rate leads to a decrease in anodic undercutting at the filament head. Experiments are underway to confirm this phenomena.

The absence of replated Cu minimizes the rate of the ORR This is also the case in the absence of oxygen.[37] Hence, using the information provided in this publication it can be speculated that any inhibitor

that limits Cu replating and/or inhibits ORR can improve resistance to scribe-creep. Consider chromate ions, for example, which inhibit scribe-creep in the same type of test. It has been shown that the presence of chromate ions inhibits open-circuit potential corrosion and Al_2CuMg dissolution (anodic inhibition), reduces pitting (anodic inhibition), and inhibits cathodic ORR (cathodic inhibition).[23-24] Therefore, one beneficial role of chromate during scribe-creep can be interpreted through its role in minimizing Cu replating. The other is the well-known effect of enhanced adhesion.[23-25] However, the suppression of the dissolution of the Al-Cu-Mg-type constituent particles under paints should not be underestimated, since this function, in turn, will decrease the amount of Cu redeposition that is necessary to enhance ETR rates for oxygen reduction. The presence of chromate not only inhibits the dissolution of the Al-Cu-Mg-type IMC but also suppresses the ORR rate on AA2024-T3 and the remaining Al-Cu and Al-Cu-Mn-Fe-type IMC.[23-24]

Therefore, alternative pretreatments, coating inhibitors, or alloy compositions that minimize the propensity for Cu replating should all be capable of reducing underpaint corrosion rates implicated in scribe-creep measurements on AA2024-T3. For instance, a hydrotalcite pigment containing an ORR inhibiting anion might inhibit ORR reactions, as shown by Kendig and Hon,[88] and reduce scribe-creep rates via this mechanism. Inhibitors may function in other ways such as by limiting anodic dissolution, buffering pH, or gettering Cl^-,[35,89-90] but, clearly, modifying Cu replating and suppressing the rate of the ORR are important mechanisms of the inhibition of scribe-creep.

CONCLUSIONS

❖ Cyclic voltammetry to assess Cu redox processes indicates that exposure to NaCl solutions and NaOH pretreatment significantly increases redeposited Cu on bare surfaces of AA2024-T3. Cathodic E-log I confirms enhancement of the charge-transfer-controlled ORR with Cu replating.

❖ Cyclic voltammetric tests indicate that NaOH + HNO_3 pretreatment produces a surface that exhibits low levels of Cu redeposition and resists further redeposition during scribe-creep tests on organically coated AA2024-T3.

❖ Scribe-creep rates on coated AA2024-T3 after all pretreatments were faster than those observed on high-purity Al and were accelerated by temperature. However, at 50°C all three pretreatments on AA2024-T3 showed high scribe-creep lengths and growth rates.

❖ As a first approximation, the rate of scribe-creep follows a simple Arrhenius-type, thermally activated growth rate behavior, but the growth rate decreases with time in a complex manner given by $l \propto t^n$, where $n \sim 1/2$. The activation energies observed are consistent with the notion that the scribe-creep process, in this instance, is controlled by the ETR associated with oxygen reduction in the charge and mixed charge-mass-transport-controlled regimes.

❖ Coated AA2024-T3, with large amounts of replated Cu and/or a large capacity for replating Cu, exhibited the largest increase in scribe-creep rate with increasing temperature. Scribe-creep rates could, therefore, be predicted based on prior Cu redeposition and the propensity for Cu redeposition.

ACKNOWLEDGMENTS

This work was supported by the Air Force Office of Scientific Research (AFOSR) Grant no. F49620-02-1-0301 under the supervision of Dr. P.C. Trulove and Dr. J. Gresham.

REFERENCES

1. R.G. Buchheit, J. Electrochem. Soc. 142 (1995): p. 3,994.
2. R.G. Buchheit, R.P. Grant, P.F. Hlava, B. McKenzie, G.L. Zender, J. Electrochem. Soc. 144 (1997): p. 2,621-2,628.
3. G.S. Chen, M. Gao, R.P. Wei, Corrosion 52 (1996): p. 8-15.
4. G.S. Chen, C.-M. Liao, K.-C. Wan, M. Gao, R.P. Wei, “Effects of Environment on Initiation of Crack Growth,” eds. W.A. Van Der Sluys, R.S. Piascik, R. Zawierucha, ASTM STP 1298 (West Conshohocken, PA: ASTM International, 1997), p. 18.
5. M.A. Alodan, W.H. Smyrl, J. Electrochem. Soc. 144 (1997): p. L282-L284.
6. M.A. Alodan, W.H. Smyrl, J. Electrochem. Soc. 145 (1998): p. 1,571.
7. M. Büchler, J. Kerimo, F. Guillaume, W.H. Smyrl, J. Electrochem. Soc. 147 (2000): p. 3,691.
8. M.J. Pryor, D.S. Keir, J. Electrochem. Soc. 102 (1955): p. 605.
9. J.R. Scully, T.O. Knight, R.G. Buchheit, D.E. Peebles, Corros. Sci. 35 (1993): p. 185-195.
10. P. Schmutz, G.S. Frankel, J. Electrochem. Soc. 145 (1998): p. 2,295.
11. R.G. Buchheit, L.P. Montez, M.A. Martinez, J. Michael, J. Hlava, J. Electrochem. Soc. 146 (1999): p. 4,426.
12. V. Guillaumin, G. Mankowski, Corros. Sci. 41 (1999): p. 421-438.
13. T. Suter, R.C. Alkire, “Microelectrochemical Studies of Pit Initiation at Single Inclusions in a 2024-T3 Al Alloy,” in Critical Factors in Localized Corrosion III, PV 98-17 (Boston, MA: The Electrochemical Society, 1998), p. 118-129.
14. C. Blanc, B. Lavelle, G. Mankowski, Corros. Sci. 39 (1997): p. 495-510.
15. R.R. Leard, R.G. Buchheit, Mater. Sci. Forum 396-402 (2002): p. 1,491-1,496.
16. R.G. Buchheit, R.K. Boger, “Cu Redistribution and Surface Enrichment Due to Dissolution of Al-Cu Alloys,” CORROSION/2001 Research Topical Symposium—Localized Corrosion, 265-292 (Houston, TX: NACE International, 2001), p. 265-292.
17. K. Sieradski, N. Dimitrov, “Evolution of Localized Corrosion in Al Alloy 2024-T3,” NACE Topical Research Symposium Proc. (Houston, TX: NACE, 2001), p. 293-299.
18. N. Dimitrov, J.A. Mann, K. Sieradski, J. Electrochem. Soc. 146 (1999): p. 98-102.
19. N. Dimitrov, J.A. Mann, M.B. Vukmirovic, K. Sieradski, J. Electrochem. Soc. 148 (2000): p. 3,283.
20. M.B. Vukmirovic, N. Dimitrov, K. Sieradski, J. Electrochem. Soc. 149 (2002): p. B428.
21. G.O. Ilevbare, J.R. Scully, J. Yuan, R.G. Kelly, Corrosion 56 (2000): p. 227-242.
22. O. Schneider, G.O. Ilevbare, R.G. Kelly, J.R. Scully, “In-Situ Confocal Laser Scanning Microscopy Surface Metrology Studies of Corrosion on AA 2024-T3,” in Corrosion and Corrosion Prevention of Low-Density Metals and Alloys, PV 2000-23 (Pennington, NJ: The Electrochemical Society, 2000), p. 87-100.
23. J.V. Kloet, W. Schmidt, A.W. Hassel, M. Stratmann, Electrochim. Acta 49 (2004): p. 1,675-1,685.
24. G.O. Ilevbare, J.R. Scully, Corrosion 57 (2001): p. 134-152.
25. L. Fedrizzi, F. Deflorian, S. Rossi, P.L. Bonora, Mater. Sci. Forum 289-292 (1998): p. 485-498.

26. J.R. Scully, D.E. Peebles, A.D. Romig, Jr., D.R. Frear, C.R. Hills, Metall. Mater. Trans.-A, vol. 23A (1992): p. 2,641-2,655.
27. R.G. Buchheit, "Conversion Coating Formation on Aluminum by Inhibited Alkaline Solutions," in Environmentally Acceptable Inhibitors and Coatings, PV 95-16 (Pennington, NJ: The Electrochemical Society, 1995), p. 133-145.
28. M. Rohwerder, E. Hornung, M. Stratmann, Electrochim. Acta 48 (2003): p. 1,235-1,243.
29. F. Mansfeld, Y. Wang, S.H. Lin, "Surface Modification of High-Copper Aluminum Alloys," in Environmentally Acceptable Inhibitors and Coatings, PV 95-16 (Pennington, NJ: The Electrochemical Society, 1995), p. 169-180.
30. T.P. Hoar, Filiform Corrosion and Related Phenomena, Society of Chemical Industry-Corrosion Group 46 (London, U.K.: Chem. Ind., 1952), p. 1,126-1,127.
31. A. Bautista, Prog. Org. Coat. 28 (1996): p. 49-58.
32. H. Kaesche, Werkst. Korros. 11 (1959): p. 668-681.
33. H.J.W. Lenderink, "Filiform Corrosion of Coated Aluminum Alloys—A Study of Mechanisms" (Ph.D. diss., Technische Universiteit Delft, 1995).
34. R.T. Ruggeri, T.R. Beck, Corrosion 39 (1983): p. 452-465.
35. G. Williams, H.N. McMurray, J. Electrochem. Soc. 150 (2003): p. B380-B388.
36. G. Williams, H.N. McMurray, Electrochem. Comm. (2003): p. 871-877.
37. W. Schmidt, M. Stratmann, Corros. Sci. 40 (1998): p. 1,441-1,443.
38. J.V. Kloet, W. Schmidt, A.W. Hassel, M. Stratmann, "Investigations into the Role of Copper in AA2024-T3 Aluminum Alloys on Filiform Corrosion Advancement and the Role of Chromium in Corrosion Inhibition," 2001 AFOSR Corrosion Review (Duck Key, FL: AFOSR, 2001).
39. H. Leth-Olsen, K. Nisancioglu, Corrosion 53 (1997): p. 705.
40. L.F. Vega, "Influence of Surface Treatments on Durability of Painted Al Alloys," paper no. 970731, SAE Technical Paper Series—International Congress & Exposition (Warrendale, PA: SAE International, 1997).
41. L.F. Vega, F. Bovard, T. Nakayama, K. Ikeda, H. Shige, E.L. Colvin, "Filiform Corrosion of Aluminum Alloys: Influence of Alloy Composition," NACE Topical Research Symposium Proc. (Houston, TX: NACE, 2000), p. 149-160.
42. P. Ziman, E.L. Colvin, J.J. Witters, "Corrosion Performance Comparison of Bare and Alclad 2024-T3 Sheet in Painted and Unpainted Conditions," Alcoa Technical Report, 1996.
43. G.M. Hoch, "A Review of Filiform Corrosion," in Localized Corrosion NACE-3 (Houston, TX: NACE, 1974).
44. Y. Komatsu, New Pretreatment and Painting Technology for All Aluminum Automotive Body, paper no. 910787, SAE Technical Paper Series—International Congress/AIRP Meeting (Warrendale, PA: SAE International, 1991).
45. F. Mansfeld, M.W. Kendig, S. Tsai, Corrosion 38 (1982): p. 478-485.
46. M.W. Kendig, A.T. Allen, S.L. Jeanjaquet, F. Mansfeld, "Application of Impedance Spectroscopy to the Evaluation of Corrosion Protection by Inhibitors and Polymer," CORROSION/85, paper no. 85074 (Houston, TX: NACE, 1985).
47. A. Afseth, J.H. Nordlien, G.M. Scamans, K. Nisancioglu, Corros. Sci. 43 (2001): p. 2,359-2,377.
48. X. Zhou, G.E. Thompson, G.M. Scamans, Corros. Sci. 45 (2003): p. 1,767-1,777.
49. J.M.C. Mol, B.R.W. Hinton, D.H. Van Der Weijde, J.H.W. De Wit, S. van der Zwaag, J. Mater. Sci. 35 (2000): p. 1,629-1,639.
50. J.M.C. Mol, A.E. Hughes, B.R.W. Hinton, S. van der Zwaag, Corros. Sci. 46 (2004): p. 1,201-1,224.
51. A.E. Hughes, J.M.C. Mol, B.R.W. Hinton, S. van der Zwaag, Corros. Sci. 47 (2005): p. 107-124.
52. E.E. Underwood, Quantitative Stereology (Reading, MA: Addison-Wesley Publishing Company, 1970), p. 123-126.
53. E.E. Underwood, "Applications of Quantitative Metallography," vol. 8, Metallography, Structures, and Phase Diagrams, eds. T. Lyman, H.E. Boyer, W.J. Carnes, M.W. Chevalier, E.A. Durand, P.M. Unterweiser, H. Baker, P.D. Harvey, H.L. Waldorf, H.V. Bukovics, C.W. Kirkpatrick, J.W. Kothera (Materials Park, OH: ASM International, 1973), p. 37-47.
54. B.D. Ripley, "Spatial Statistics," in Wiley Series in Probability and Mathematical Statistics (New York, NY: John Wiley and Sons, 1981), p. 145-190.
55. P.J. Diggle, "Statistical Analysis of Spatial Point Patterns," in Mathematics in Biology, eds. R. Sibson, J.E. Cohen (New York, NY: Academic Press Inc., 1983), p. 70-89.
56. A.J. Davenport, B. Liu, "Copper Accumulation During Cleaning of Al-Cu Alloys," Electrochemical Society Proc., PV 2000-23 (Pennington, NJ: The Electrochemical Society, 2000), p. 41-46.
57. A. Afseth, J.H. Nordlien, G.M. Scamans, K. Nisancioglu, Corros. Sci. 44 (2002): p. 2,491-2,506.
58. A. Afseth, J.H. Nordlien, G.M. Scamans, K. Nisancioglu, Corros. Sci. 44 (2002): p. 2,543-2,559.
59. H. Leth-Olsen, K. Nisancioglu, Corros. Sci. 40 (1998) p. 1,179-1,194.
60. M.A. Jakab, F. Presuel-Moreno, J.R. Scully, Corrosion 61 (2005): p. 246.
61. M.A. Jakab, D.A. Little, J.R. Scully, J. Electrochem. Soc. 152 (2005): p. B311-B320.
62. ASTM B 117, "Standard Practice for Operating Salt Spray (Fog) Apparatus," in Annual Book of ASTM Standards, vol. 03.02 (West Conshohocken, PA: ASTM International, 1997), p. 1-8.
63. E.L. Colvin, L.F. Vega, M.W. Egbert, T. Nakayama, K. Ikeda, H. Shige, T. Ueda, M. Inman, "Filiform Corrosion of Aluminum Auto Body Sheet in Accelerated and Outdoor Environments," paper no. 970735, SAE Technical Paper Series—International Congress & Exposition (Warrendale, PA: SAE International, 1997), p. 69-83.
64. K.S. Ferrer, R.G. Kelly, Corros. Sci. 57 (2001): p. 110-117.
65. A. Ackermann, Kolloid-Zeitschrift: Zeitschrift fèur Reine und Angewandte Kolloidwissenschaft 28 (1921): p. 270-281.
66. A. Ackermann, Kolloid-Zeitschrift: Zeitschrift fèur Reine und Angewandte Kolloidwissenschaft 59 (1932): p. 49-55.
67. W. Funke, Prog. Org. Coat. 9 (1981): p. 29-46.
68. H. Haagen, K. Gaszner, K. Scheck, Farbe Lack 97 (1991): p. 306-310.
69. C. Hahin, R.G. Buchheit, "Filiform Corrosion," in ASM Handbook—Corrosion: Fundamentals, Testing, and Protection, vol. 13A, eds. S.D. Cramer, B.S. Covino, Jr. (Materials Park, OH: ASM International, 2003), p. 248-256.
70. M. Iwata, Y. Itoi, E. Sato, J. Jpn. Inst. Light Met. 34 (1984): p. 273-277.
71. M. Iwata, M. Nishikado, E. Sato, Y. Itoi, J. Jpn. Inst. Light Met. 34 (1984): p. 531-536.
72. J.P. Rique, Surfaces 17 (1978): p. 55-58.
73. C.F. Sharman, Nature 153 (1944): p. 621-622.
74. W.H. Slabaugh, E.J. Chan, J. Paint Technol. 38 (1966): p. 417-420.
75. W.H. Slabaugh, W. Dejager, S.E. Hoover, L.L. Hutchinson, J. Paint Technol. 44 (1972): p. 76-83.
76. H.E. Townsend, Corrosion 52 (1996): p. 66-71.
77. M. Van Loo, D.D. Laiderman, R.R. Bruhn, Corrosion 9 (1953): p. 277-283.
78. J.M. Williams, "Mechanistic Framework of Localized Coating Failure on Copper-Containing Aluminum Alloys AA2024-T3 and AA1100-H14" (Master's thesis, University of Virginia, 2002).
79. G. Grundmeier, W. Schmidt, M. Stratmann, Electrochim. Acta 45 (2000): p. 2,515-2,533.
80. E.H. Hollingsworth, H.Y. Hunsicker, "Corrosion of Aluminum and Aluminum Alloys," in Metals Handbook, 9th ed., vol. 13 Corrosion, eds. J.R. Davis, J.D. Destefani, H.J. Frissell, G.M. Crankovic (Materials Park, OH: ASM International, 1987), pp. 33-126, 583-609.
81. J. Crank, G.S. Park, Diffusion in Polymers, eds. J. Crank, G.S. Park (New York, NY: Academic Press, 1968), p. 5.
82. R.M. Barrer, Trans. Faraday Soc. 35 (1939): p. 628.
83. H. Leidheiser, E.M. Allen, F.M. Fowkes, R.D. Granata, J.F. McIntyre, J.A. Manson, "Corrosion Control Through a Better Understanding of the Metallic Substrate/Organic Coating/Interface," in The Effect of Temperature and Alkali Metal Cation on the Cathodic Delamination of Polybutadiene from Steel, eds. H. Leidheiser, J. Catino (Bethlehem, PA: Lehigh University, 1986), p. 21-27.
84. R. Stannett, ed., Diffusion in Polymers (New York, NY: Academic Press, 1968), p. 41.
85. J.H. Wang, C.V. Robinson, I.S. Edelman, J. Am. Chem. Soc. 75 (1953): p. 466.
86. G.J. Van Amerongen, J. Polym. Sci. 5 (1950): p. 307.
87. C.H. Hamann, A. Hamnett, W. Vielstich, Electrochemistry (New York, NY: Wiley-VCH, 1998).
88. M.W. Kendig, M. Hon, Electrochem. Solid-State Lett. 8 (2005): p. B10-B11.
89. G. Williams, H.N. McMurray, J. Electrochem. Soc. 148 (2001): p. B377-B385.
90. G. Williams, H.N. McMurray, Electrochem. Solid-State Lett. 6 (2003): p. B9-B11.